Mini-Jets in Deep Inelastic Scattering at HERA

H1 Collaboration

Abstract

The production of jets with low P_T, mini-jets, in deep inelastic electron-proton scattering is studied. The analyses uses data taken with the H1 detector at HERA during the years 1999 to 2000. Mini-jet multiplicities are presented as a function of the P_T of the leading jet in bins of η and Q^2. The analysis is performed for an inclusive jet sample, and for a dijet sample, where the second jet is required to have an azimuthal angle larger than 140 degrees with respect to the leading jet. The dijet sample is split into two samples which are enhanced in direct photon and resolved photon processes, respectively. The results are compared to various QCD based models.

1   Introduction

In electron-proton scattering the partonic content of the exchanged virtual photon may be resolved if the P_T of the interacting partons is larger than Q^2 and thereby the photon will behave like a hadronic object. Thus, similar to hadron-hadron scattering there will be a certain probability that collisions between the resolved photon and the proton involve more than one parton interaction, multiple interactions (MI). Previous measurement in photoproduction at HERA [1] have shown that only models with MI give a satisfactory description of the data. This analysis constitutes the first study of possible MI in DIS from measurements of low P_T jets produced in addition to the leading jet(s) of the event.

2   Analysis method

The basic principle of the analysis is to define regions in phase space where contributions from the final state products originating from the hard primary interaction are expected to be small. The starting point is therefore to define and isolate the leading jet(s) from the hard primary interaction and investigate the remaining regions for additional activities, which in this analysis comprise the presence of mini-jets. The basic concept follows closely the one used by the CDF collaboration at the TEVATRON [2], in which case general event parameters have been investigated. In this analysis two different event samples are studied; *inclusive jet events* and *dijet events*, of which the latter constitutes a subsample of the inclusive sample. The analysis procedure is the following:

Inclusive jet sample: The leading jet is identified and reconstructed using the k_t-algorithm [3] in the hadronic center-of-mass frame h.c.m. rest frame. The jet with the highest transverse momentum in the h.c.m. rest frame is taken as the leading jet. The leading jet axis defines the azimuthal angle $\Delta\phi^*$=0 [1]. The region $|\Delta\phi^*| < 60^o$ is defined as the 'toward region', and is expected to contain all particles belonging to the leading jet. The angular region $|\Delta\phi^*| > 140^o$ is called the 'away region'. The transverse regions, $60^o < |\phi^*| < 120^o$ are those where contributions from the primary collision should be small and the effects from additional activities should be most visible. Event by event a 'high activity'- and a 'low activity' regions are defined, depending on which region contains the most and least transverse momentum, respectively. These four regions are shown. in Figure 1

Dijet sample: The dijet sample includes events having at least two jets, where the two reconstructed jets are required to be almost back-to-back. The leading jet is again defining $\Delta\phi^*$=0, whereas the jet axis of the jet with the second highest transverse momentum, the sub leading jet, is restricted to be inside the 'away region', Figure 1b . This leaves some angular space to accommodate the transverse spread of the jet within the 'away region'.

In the inclusive sample, contributions from higher order processes are expected to be higher than in the dijet sample, where the requirement of back-to-back jets limits the phase space for additional radiation. In any case, possible contributions from initial state radiation, or higher

---

[1]Observables in the h.c.m. frame are labeled with *.

order processes, have to primarily fall into the hemisphere, which is opposite to that where the 'second' jet proceeds, in order to restore the momentum balance. In cases where a third jet ends in any of the transverse regions, this is most frequently the 'high activity region'. Thus contributions from initial or final state radiation are expected to fall primarily into the 'high activity region'. Since beam remnant interactions and multiple parton scattering to first approximation should be independent of the primary interaction, the final state products may occupy any of the regions, but should be more visible in the 'low activity region'. Finally, the difference between the 'high' and 'low' activity regions should correspond to higher order emissions.

3 Event Selection

The analysis is based on data taken with the H1 detector in 1999/2000 using colliding positrons and protons at energies of 27.5 GeV and 920 GeV, respectively. This gives a center-of-mass energy of $\sqrt{s} = 319$ GeV. The data collected corresponds to an integrated luminosity of 57.4 pb^{-1}.

Deep inelastic scattering (DIS) events are selected by requiring a highly energetic positron in the SPACAL calorimeter,

$$E_e^{'} > 9 \, \text{GeV}$$

$$156° < \theta_e < 175°,$$

where $E_e^{'}$ and θ_e is the energy and polar angle of the scattered positron, respectively. The photon virtuality, Q^2, and the inelasticity, y, are determined using the electron method [4] and must fulfill

$$5 \, \text{GeV}^2 < Q^2 < 100 \, \text{GeV}^2$$

$$0.1 < y < 0.7.$$

The invariant mass of the hadronic final state W is obtained from the relation $W^2 = Q^2(\frac{1}{x_{bj}} - 1)$ and is required to be higher than 200 GeV in the h.c.m. system, in order to enhance small x_{bj} contributions and to increase the probability of mini jet production.

The inclusive jet sample consists of events that contain at least one jet, whereas the dijet sample includes events with at least two jets. For both samples the jet with the highest transverse momentum is chosen as the leading jet and in the dijet sample the sub leading jet has to fulfill the requirement $|\Delta\phi_{ls}^*| = |\phi_{lj}^* - \phi_{sj}^*| > 140°$, where ϕ^* is the jet azimuthal angle and the labels *lj* and *sj* denotes the leading and sub leading jets, respectively. The jets are reconstructed by the inclusive k_t-algorithm [3] in its p_t weighting scheme , applied to combined object of tracks and calorimetric clusters [5] in the h.c.m. rest frame. To ensure a good jet reconstruction it is required that the leading and sub leading jets must fulfill -1.7 $< \eta^{lab} <$ 2.79 and $P_T^{(*)} > 5$ GeV. Here, the pseudo-rapidity is given by $\eta_j = -\ln(\tan(\theta_j/2))$, where θ_j is the polar angle of the

jet in the lab frame, and P_T is the transverse energy of the jet. The P_T cut is applied both in lab and h.c.m. rest frame.

Mini-jets are reconstructed with the same jet algorithm as the leading jets and within the same η^{lab} region. However, the minimum transverse momentum of a mini-jets is specified as 3 GeV both in lab and HCM frame .

4 QCD Models

Several MC generator have been used for comparisons with the data.

RAPGAP [6] includes standard leading order cross section for direct and resolved photon interactions together with initial and final state radiation obtained from the DGLAP evolution equations. RAPGAP does not include any model for multiple interactions.

ARIADNE [7] is based on the colour dipole model, CDM, to simulate the QCD parton cascade. Since the colour dipoles radiate independently there is no ordering in the transverse momenta of the emitted partons as there is in the DGLAP evolution. For these two MC programs DJANGO [8] is used to provide an interface to HERACLES [9] for radiative QED corrections.

PYTHIA6.224 generator [10,11] uses leading order α_S matrix elements supplemented by initial and final state radiation generated according to the DGLAP evolution scheme in the leading logarithm approximation. Two options are considered in this paper, PYTHIA without MI , refered to as PYTHIA, and PYTHIA including MI, denoted PYTHIA MI.

All three MC generators above describe the hadronization according to the Lund string fragmentation model using JETSET [12].

HERWIG [13–15] uses first order α_S matrix elements together with the parton-shower approach for initial- and final-state QCD radiation, including colour coherence effects and azimuthal correlations both within jets and between jets. Hadronization is performed according to the cluster hadronization model. An underlying event structure similar to that of a minimum-bias collision may be superimposed on the hard emission. In this analyses 0% and 10% probability of SUE are simulated for the resolved part, and will be refered in this paper as HERWIG and HERWIG 10%SUE respectively.

5 Correction Procedure and Systematic Uncertainties

The Data are corrected for limited detector resolution and acceptance using a bin-by-bin procedure. Correction factors are determined using detector simulated events, generated by the Monte Carlo programs RAPGAP and DJANGO with ARIADNE, where QED radiation has been taken into account. The correction factors are in the range 0.8-1.4.

The systematic uncertainties considered in this analysis are coming from the following sources:

- The systematic error from the uncertainty in the hadronic energy scale of the LAr calorimeter is 4%.

- The systematic error from the uncertainty in the hadronic energy scale of the hadronic SPACAL calorimeter is 7%.

- The uncertainty in the absolute value of the electromagnetic energy scale contributes a systematic error of around 1%.

- The momenta of charged tracks measured by the central drift chamber have an accuracy of $\pm$ 3%.

- The scattering angle of the electron is measured to an accuracy of ± 1 mrad.

- The positron energy has been varied by $\pm$ 1%

- The systematic uncertainties in the correction factors due to model dependence is the half of the difference between the correction factors obtained by RAPGAP and DJANGO.

The largest systematic uncertainties are obtained from the correction factors due to the model dependence which can be as large as 20 %. All systematic uncertainties and the statistical error are combined in quadrature to get the total error of the measurement.

6 Results

6.1 The inclusive sample

The multiplicity of mini jets, $< N_{minijet} >$, for the inclusive sample in the two η regions of the leading jet and in three bins of Q^2 are shown in Figs. 2- 7 as a function of $P_T^{(*)}$ of the leading jet. The following can be noticed:

The toward and away regions: All the different MC models, with or without MI/SUE, describe the 'toward region' well in all Q^2 bins (Figs. 2- 7, a-c), indicating that such contributions are non-significant in these regions. In the 'away region' there is an overall reasonable agreement for all models. Also in 'the away region' the difference between PYTHIA with and without MI and HERWIG with and without SUE is very small, as expected.

The high activity region: The predictions of $< N_{minijet} >$ by the MC models including no MI/SUE are generally too low in all Q^2-bins both for central and forward rapidities (Figs. 2- 7, g-i). PYTHIA+MI describes the data points fairly well in the lowest Q^2-bin and somewhat less well in the higher Q^2-bins, again for both regions in rapidity (Figs. 3,6, g-i). Adding 10% SUE to HERWIG improves the agreement with data significantly but is not quite enough to reproduce the data, especially in the central rapidity region (Figs 4,7, g-i).

The low activity region: The MC models with no MI included, significantly undershoots the data in all Q^2 bins for both forward and central rapidities (Figs. 2- 7, j-l). These deviations

4

clearly increase with decreasing Q^2-values. PYTHIA+MI gives a much better description of the data (Figs. 3,6, i-l), although the deviations are still large in the highest Q^2-bin. HERWIG 10%SUE does even better (Figs. 4,7, i-l). The behaviour of MC:s is consistent with an increased contribution from resolved photon events with decreasing Q^2, and thereby higher contributions from MI or SUE.

6.2 Dijet sample

In Figures 8- 10 $< N_{minijet} >$ is shown as a function of $P_T^{(*)}$ of the leading jet in the dijet sample, for two regions of x_γ where x_γ is the fraction of the photon energy carried by the parton involved in the hard scattering and $x_\gamma = \frac{P_{T,lj}^* \exp(\eta_{lj}^*) + P_{T,sj}^* \exp(\eta_{sj}^*)}{2E_\gamma^*}$. The following observations can be made:

The toward and away regions: As for the inclusive sample the predictions of the model are consistent with the data in both the 'torward region' (Figs. 8- 10, a-b), and in the 'away region' (Figs. 8- 10, c-d).

The high activity region: The standard QCD model predictions are closer to data for direct photon processes (Figs. 8- 10, f) than for resolved (Figs. 8- 10, e), where they are generally too low. PYTHIA tends to fall below the data points, although the inclusion of MI improves the agreement (Figs. 9, e-f). With 10% SUE, HERWIG provides a resonable description of the data for resolved processes (Fig. 10e) but fails completely to reproduce the data for direct processes (Fig. 10f).

The low activity region: Predictions of the models with no MI/SUE fall too low for resolved processes (Figs. 8- 10, g), whereas they describe direct processes much better (Figs. 8- 10, h). PYTHIA without MI also gives too low multiplicities for $x_\gamma < 0.7$ but describes the data quite well if MI is included (Fig. 9g). For $x_\gamma > 0.7$ the agreement is acceptable (Fig. 9h). HERWIG needs 10% SUE in order to reproduce the data both for resolved and direct photon processes (Figs. 10, g-h).

7 Conclusions and discussion

A study of mini jets in deep inelastic electron proton scattering has been performed with the aim of finding evidence for hadronic activities in excess to those expected from the primary interaction. An overall good description of the data in 'the toward region' and 'the away region' is given by all models for both the inclusive sample and the dijet sample, which proves that the models are able to describe the primary process. In 'the high activity region' the predictions of the models without MI/SUE are generally undershooting the data for the inclusive sample and for the dijet sample with resolved photon events. The inclusion of MI or SUE improves the agreement significantly. In 'the low activity region' the deviations between data and models with no MI/SUE is even more significant than for 'the high activity region', and again the description improves drastically if MI/SUE is considered.

References

[1] S. Aid *et al.* [H1 Collaboration], Z. Phys. C**70** (1996) 17.

    D. Acosta *et al.* [CDF Collaboration], Phys. Rev. D **65** (2002) 072005.

[2] D. Acosta *et al.* [CDF Collaboration], Phys. Rev. D **65** (2002) 072005.

[3] S. D. Ellis and D. E. Soper, Phys. Rev. D **48** (1993) 3160 [arXiv:hep-ph/9305266]

[4] S. Bentvelsen, J. Engelen and P. Kooijman, Reconstruction of (x,Q^2) and Extraction of Structure Functions in Neutral Current Scattering at HERA, in *Proc. of the Workshop on Physics at HERA. Vol. 1*, edited by W. Buchmüller and G. Ingelman, page 23, Hamburg, 1991, DESY, NIKHEF-H-92-02.

[5] M. Peez, B. Portheault and E. Sauvan, *An Energy Flow Algorithm for Hadronic Reconstruction In OO: Hadroo2*, H1 internal note (2005). H1-IN-616.

[6] H. Jung, Comput. Phys. Commun. **86** (1995) 147.

[7] L. Lonnblad, Comput. Phys. Commun. **71** (1992) 15.

[8] K. Charchula, G. A. Schuler and H. Spiesberger, Comput. Phys. Commun. **81** (1994) 381.

[9] A. Kwiatkowski, H. Spiesberger and H. J. Mohring, Comput. Phys. Commun. **69** (1992) 155.

[10] T. Sjostrand, Comput. Phys. Commun. **82** (1994) 74.

[11] T. Sjostrand, Phys. Lett. B **157** (1985) 321.

[12] B. Andersson, G. Gustafson, G. Ingelman and T. Sjostrand, Phys. Rept. **97** (1983) 31.

[13] G. Marchesini and B. R. Webber, Nucl. Phys. B **310** (1988) 461.

[14] I. G. Knowles, Nucl. Phys. B **310** (1988) 571.

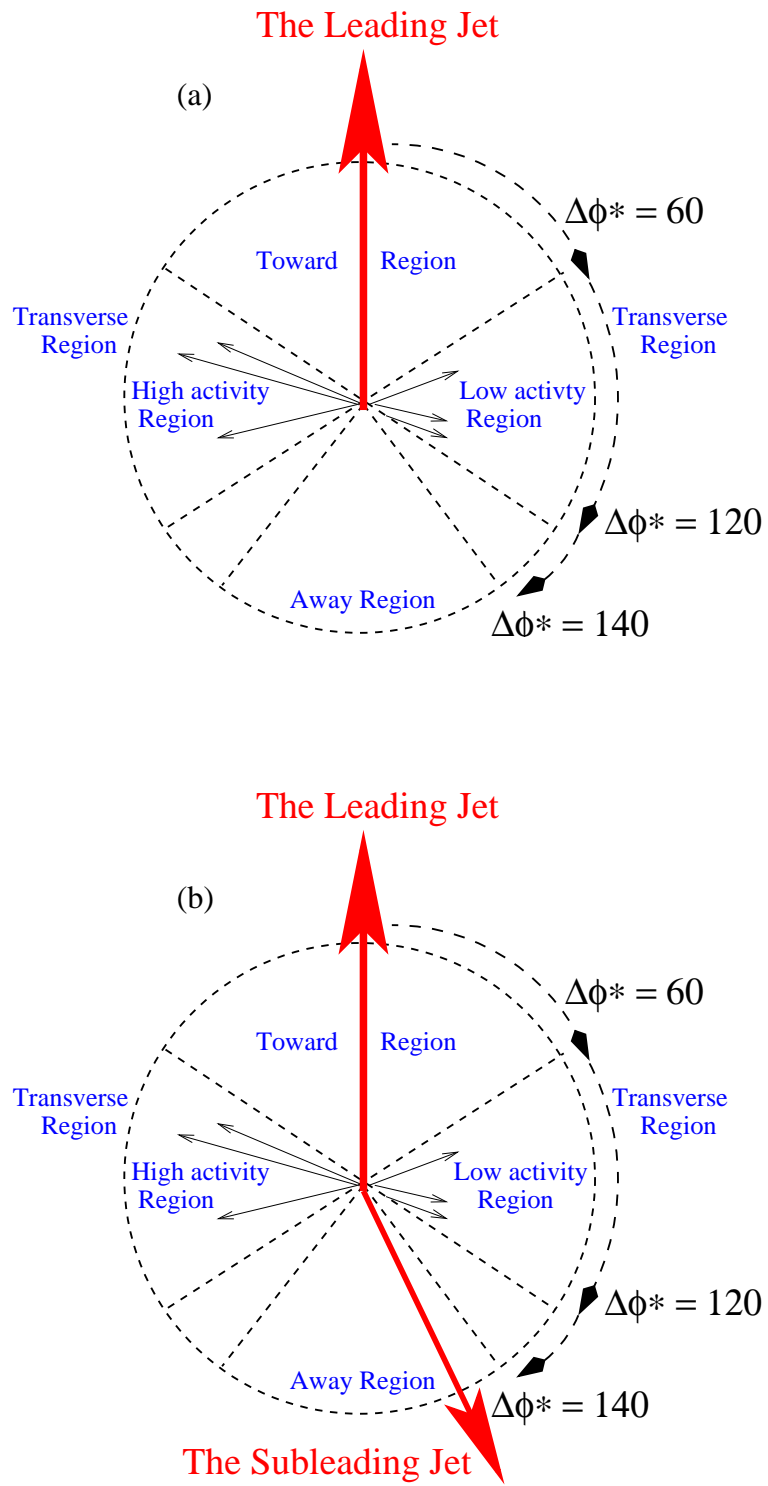[15] S. Catani, B. R. Webber and G. Marchesini, Nucl. Phys. B **349** (1991) 635.

(a)

The Leading Jet

$\Delta\phi* = 60$

Toward   Region

Transverse
Region

Transverse
Region

High activity
Region

Low activty
Region

$\Delta\phi* = 120$

Away Region

$\Delta\phi* = 140$

(b)

The Leading Jet

$\Delta\phi* = 60$

Toward   Region

Transverse
Region

Transverse
Region

High activity
Region

Low activity
Region

$\Delta\phi* = 120$

Away Region

$\Delta\phi* = 140$

The Subleading Jet

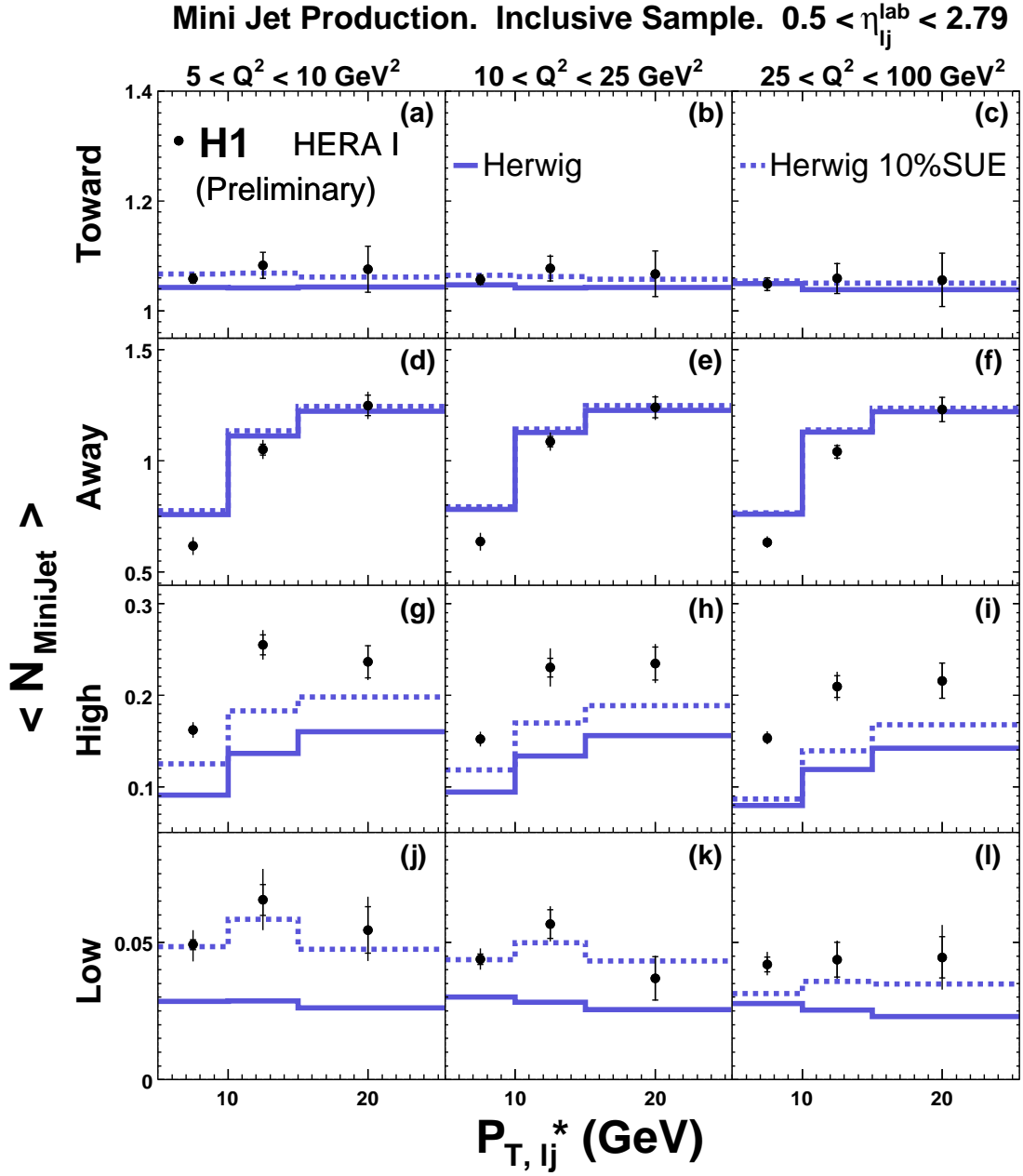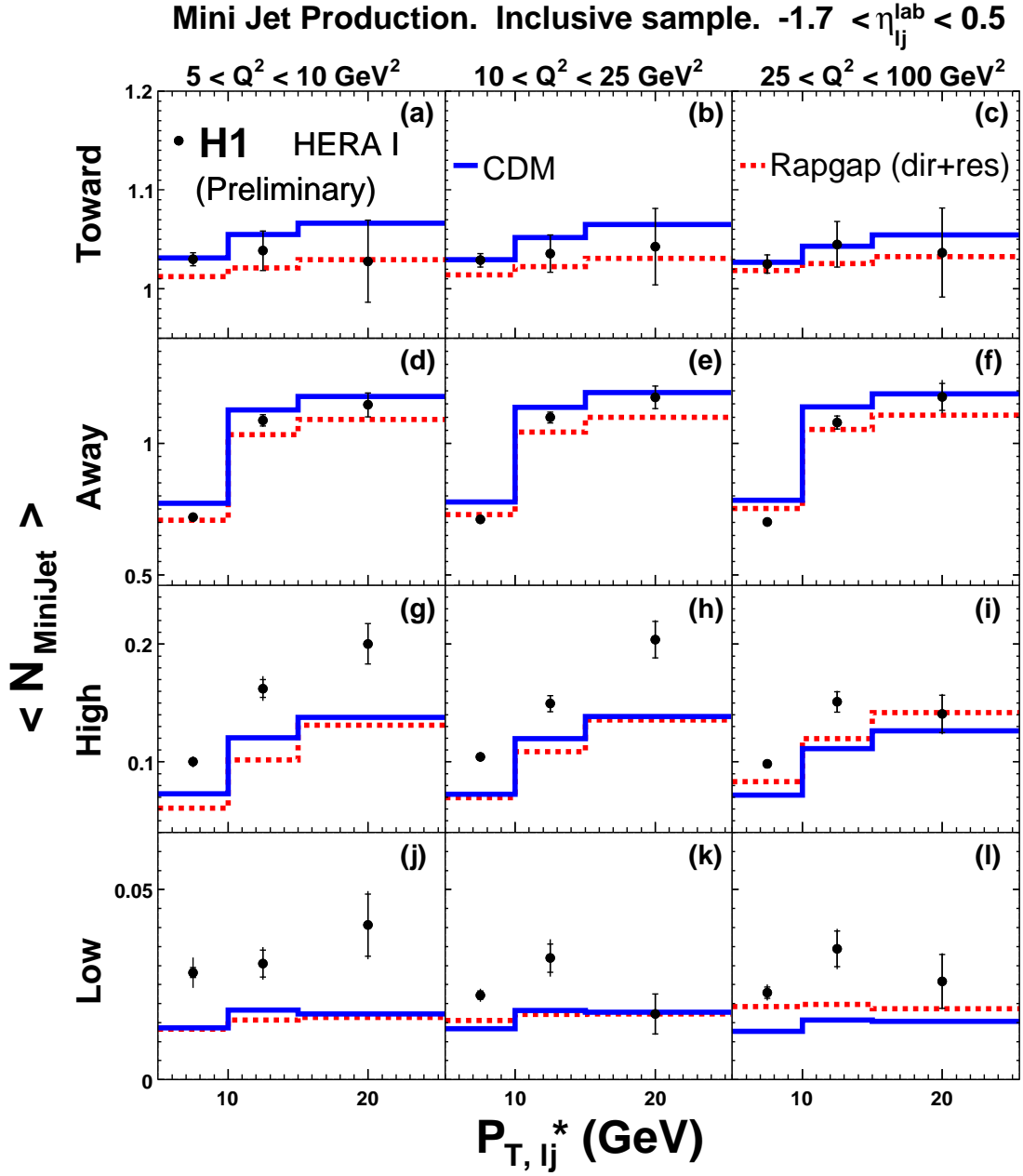Figure 1: *The transverse regions, Toward and Away regions orientation.*
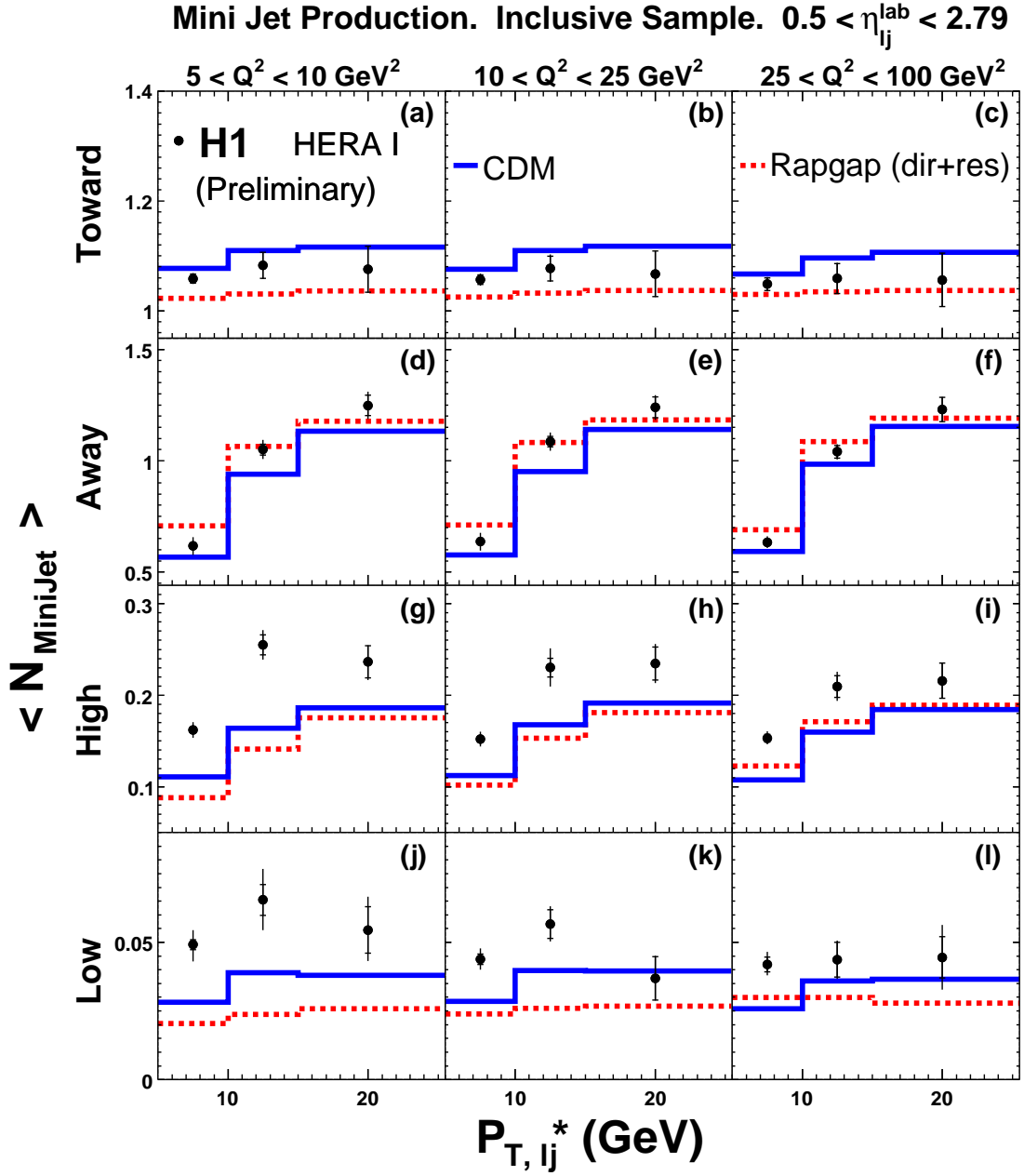
Figure 2: *The average mini-jet multiplicity at the different $\Delta\phi^*$ regions in bins of Q^2 as a function of P_T^* of the leading jet for the inclusive jet sample. The data is compared with the CDM model (solid line) and Rapgap (dashed line).*
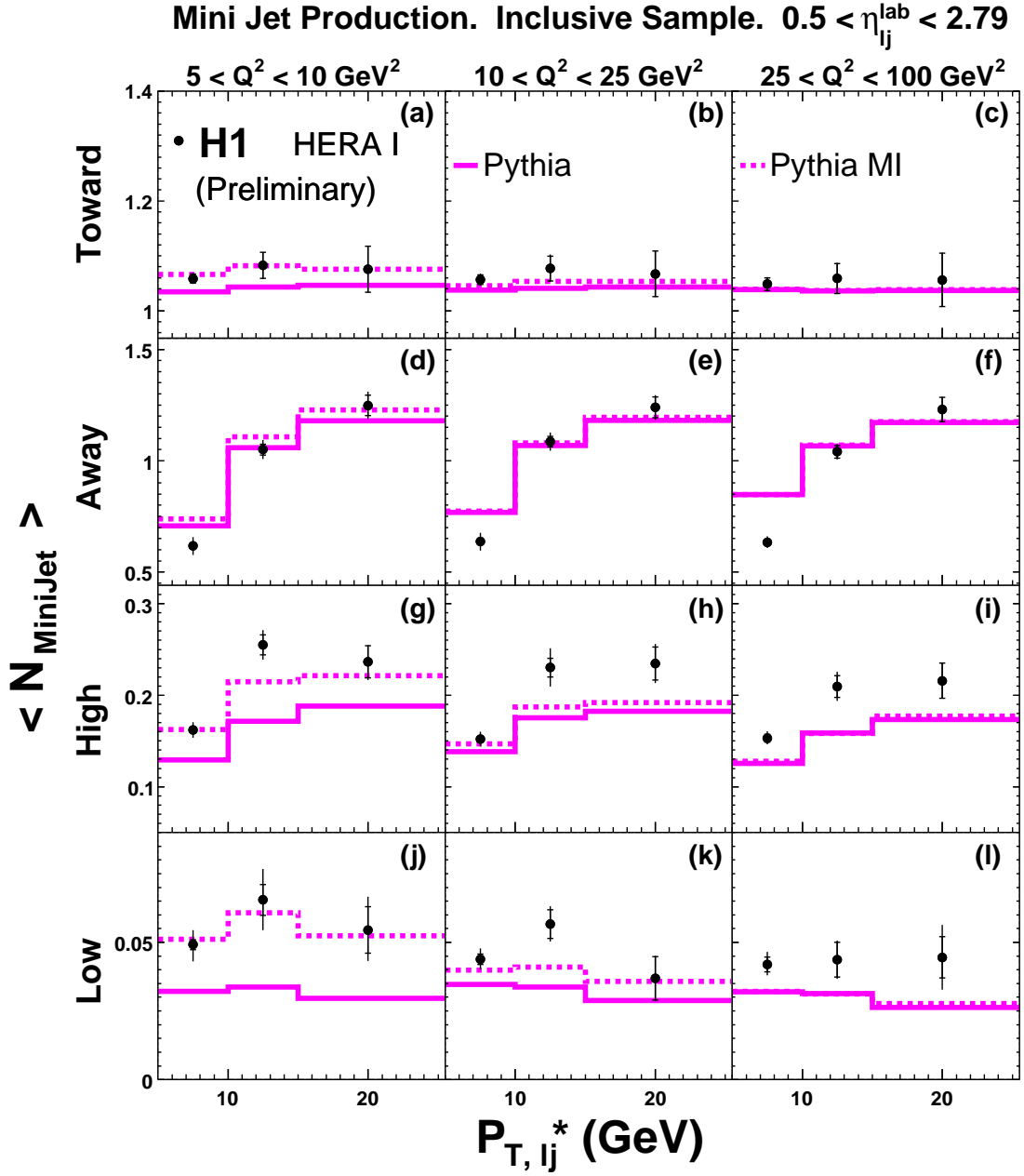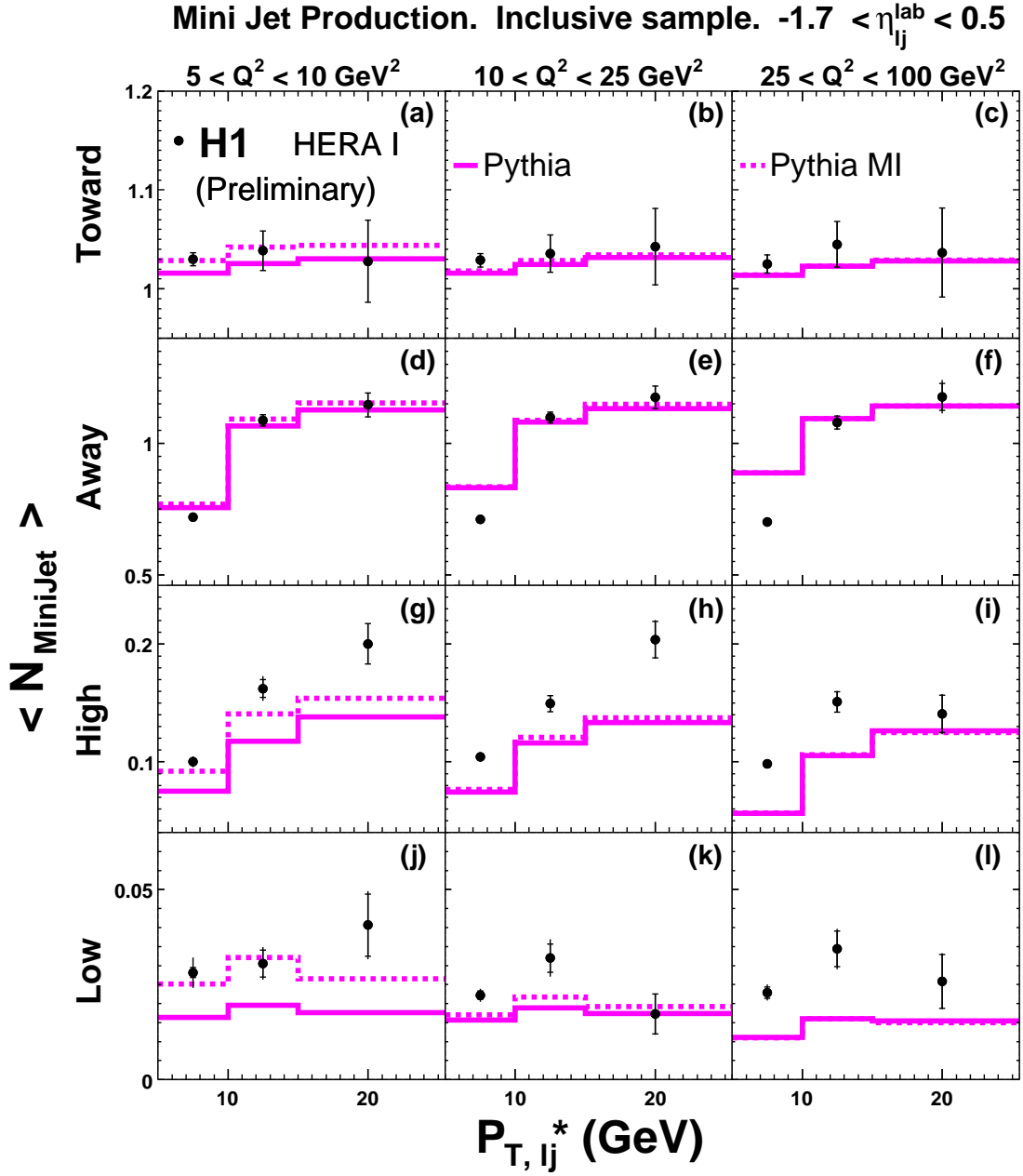
Figure 3: *The average mini-jet multiplicity at the different $\Delta\phi^*$ regions in bins of Q^2 as a function of P_T^* of the leading jet for the inclusive jet sample. The data is compared with Pythia (solid line) and Pythia with MI (dashed line).*

Figure 4: *The average mini-jet multiplicity at the different $\Delta\phi^*$ regions in bins of Q^2 as a function of P_T^* of the leading jet for the inclusive jet sample. The data is compared with Herwig (solid line) and Herwig 10%SUE (dashed line).*

Figure 5: *The average mini-jet multiplicity at the different $\Delta\phi^*$ regions in bins of Q^2 as a function of P_T^* of the leading jet for the inclusive jet sample. The data is compared with the CDM model (solid line) and Rapgap (dashed line).*

Figure 6: *The average mini-jet multiplicity at the different $\Delta\phi^*$ regions in bins of Q^2 as a function of P_T^* of the leading jet for the inclusive jet sample. The data is compared with Pythia (solid line) and Pythia with MI (dashed line).*
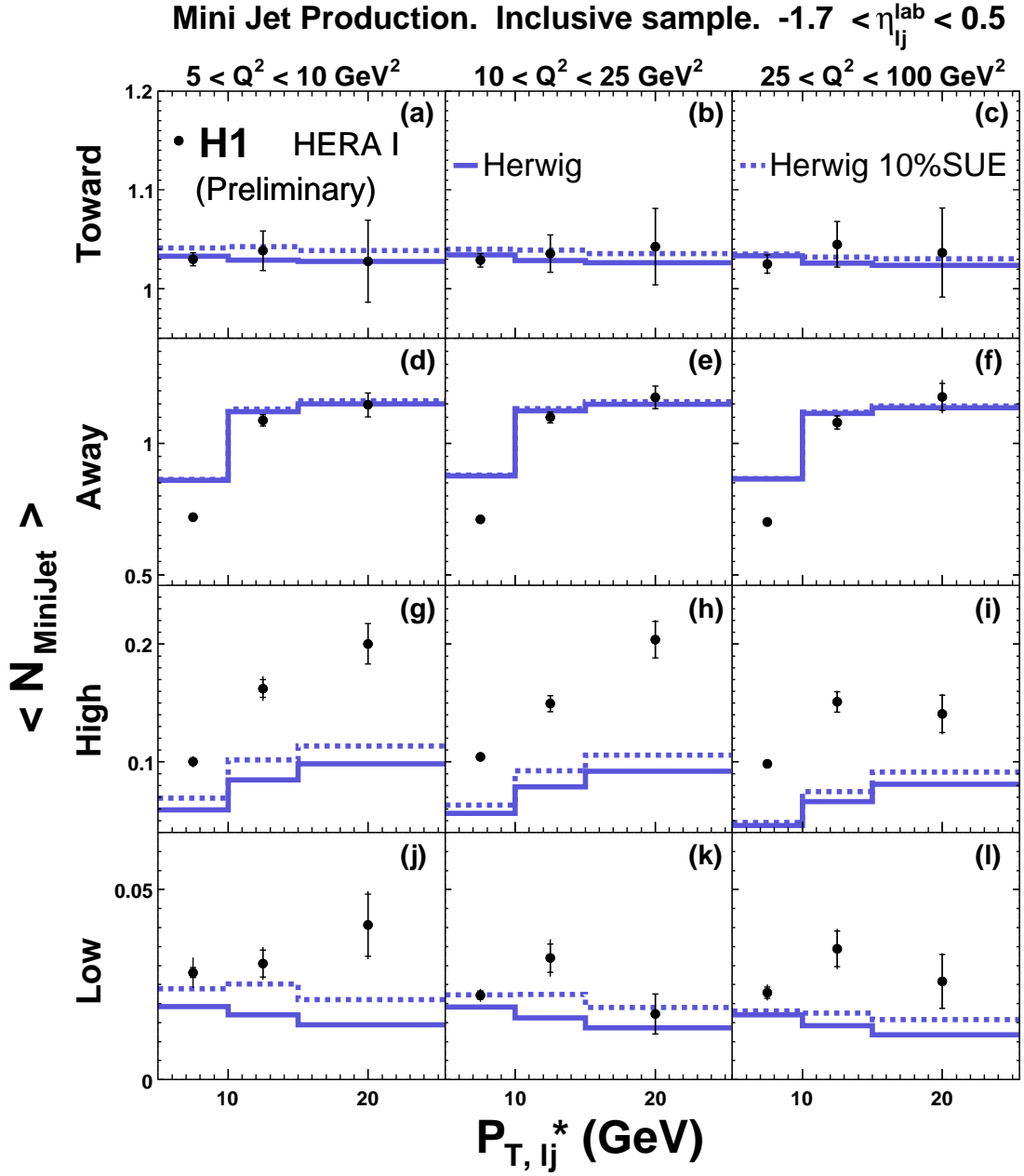
Figure 7: *The average mini-jet multiplicity at the different $\Delta\phi^*$ regions in bins of Q^2 as a function of P_T^* of the leading jet for the inclusive jet sample. The data is compared with Herwig (solid line) and Herwig 10%SUE (dashed line).*
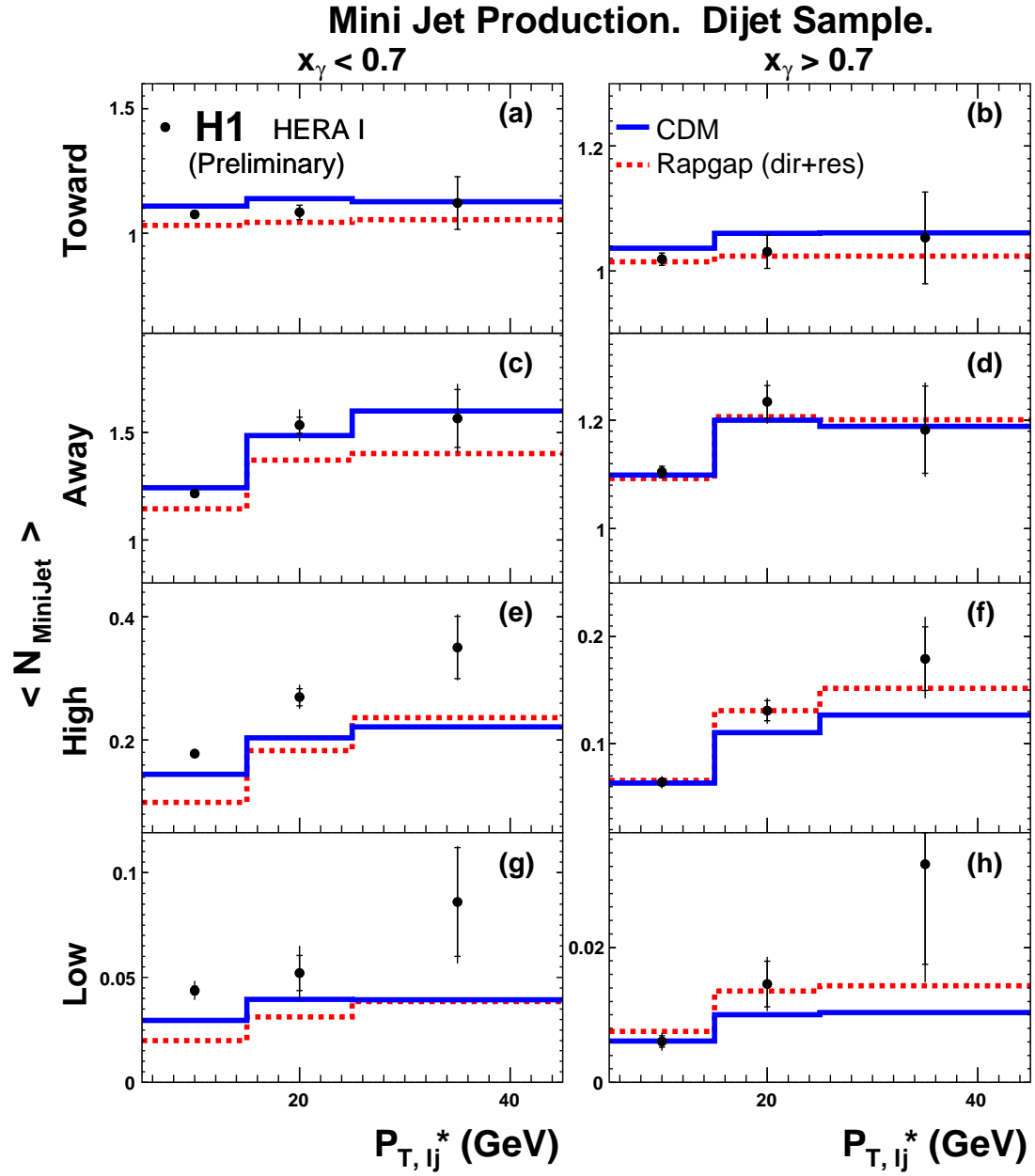
Mini Jet Production. Dijet Sample.

Figure 8: *The average mini-jet multiplicity at the different $\Delta\phi^*$ regions in bins of Q^2 as a function of P_T^* of the leading jet for the Dijet sample. The data is compared with the CDM model (solid line) and Rapgap (dashed line).*
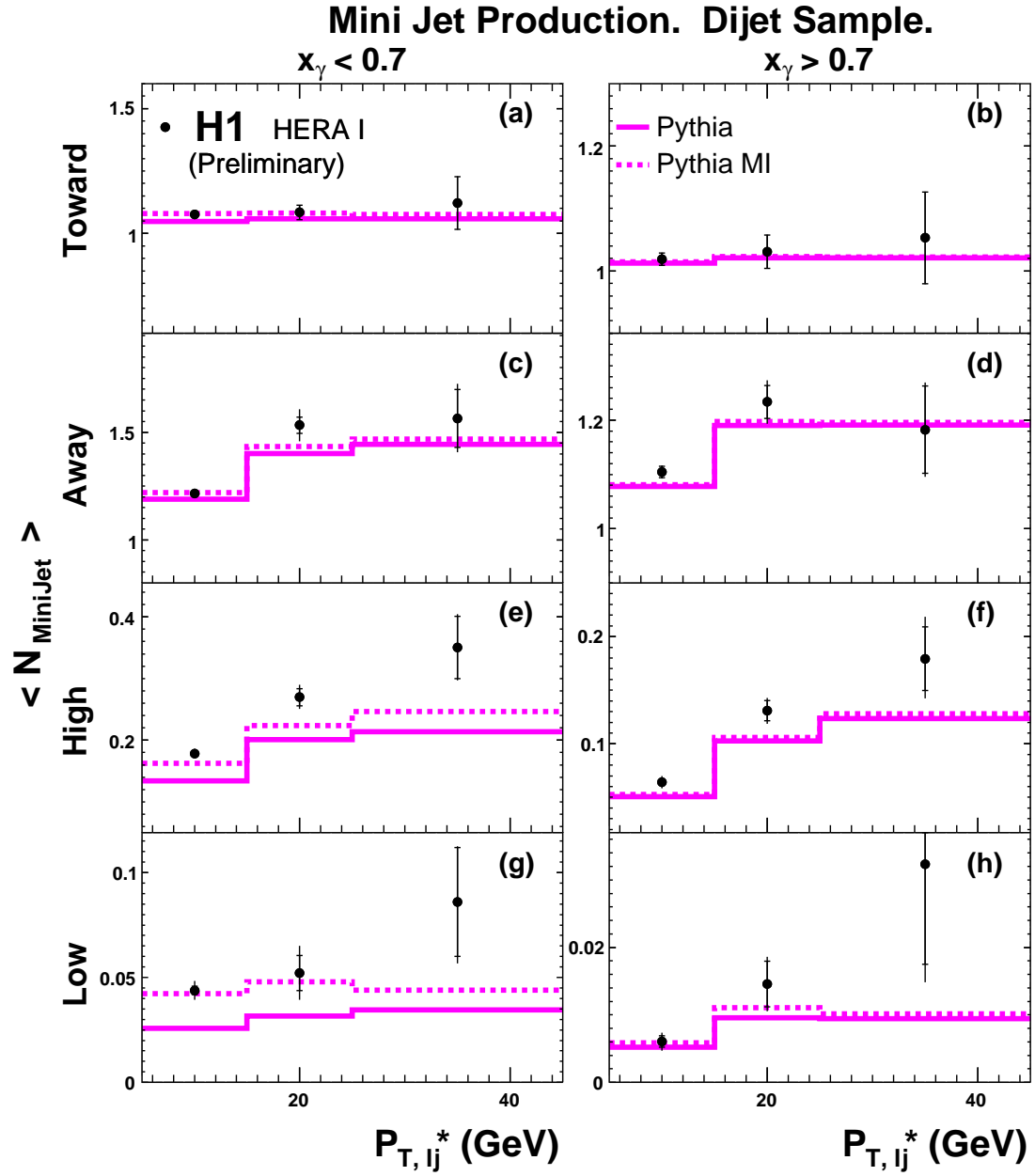
Figure 9: *The average mini-jet multiplicity at the different $\Delta\phi^*$ regions in bins of Q^2 as a function of P_T^* of the leading jet for the Dijet sample. The data is compared with Pythia (solid line) and Pythia with MI (dashed line).*
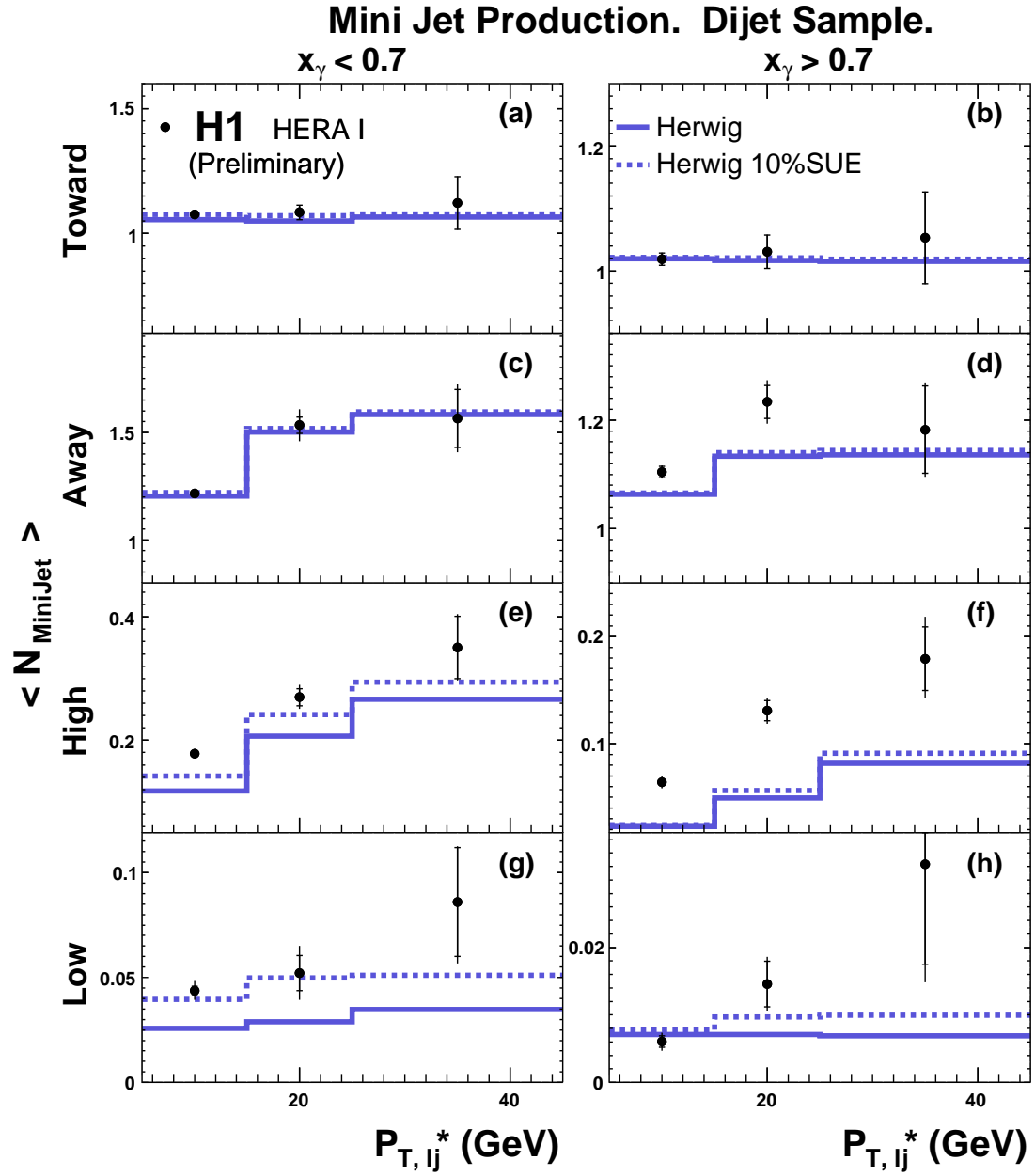
Figure 10: *The average mini-jet multiplicity at the different $\Delta\phi^*$ regions in bins of Q^2 as a function of P_T^* of the leading jet for the Dijet sample. The data is compared with Herwig (solid line) and Herwig 10%SUE (dashed line).*

16